Tribology Letters, Vol. 18, No. 3, March 2005 (© 2005)
DOI: 10.1007/s11249-004-3204-2

Investigations of microstructures and defect structures in wear affected region created on Nimonic 80A during high temperature wear

H.L. Du[a,*], P.K. Datta[a], I.A. Inman[a], E. Kuzmann[b], K. Süvegh[c], T. Marek[b] and A. Vértes[b,c]

[a]*Advanced Materials Research Institute, Northumbria University, Newcastle upon Tyne, NE1 8ST, UK*
[b]*Research Group of Nuclear Methods in Structural Chemistry HAS, Eötvös University, Budapest, Hungary*
[c]*Department of Nuclear Chemistry, Eötvös Loránd University, Budapest, Hungary*

Received 11 May 2004; accepted 21 November 2004

The microstructures of a wear induced surface glazed layers formed during sliding wear of Nimonic 80A against Stellite 6 at 20–750 °C using a speed of 0.314 m s^{-1} under a load of 7 N have been investigated using X-ray diffraction analysis (XRD), scanning electron microscopy (SEM), and transmission electron microscopy (TEM) in combination with energy dispersive X-ray (EDX) analysis. The defects formed in the glazed layers were measured by positron lifetime spectroscopy. The results indicate the formation of a wear resistant nanostructured glazed layer. Positron lifetime and Doppler-broadening measurements demonstrated that the defects (mainly dislocations) existed in the glazed layers at low temperatures which increasing wear test temperature led to decrease in defects density. Positron measurements also suggested that, at the annealing temperature (1200 °C), the presence of dislocations might lead to the formation of ordered or partially ordered regions in Nimonic 80A.

KEY WORDS: wear, glaze layer, oxidation, superalloy, Mössbauer, positrons annihilation

1. Introduction

Development of wear resistant surface glazes during the processes of high temperature wear is well documented [1–6]. Although the phenomenon of glaze formation and the associated issues of oxidation, debris generation and elemental transfer between the contacting surfaces have been studied [7–11], it is still difficult to identify the precise conditions and materials systems, which promote the formation of glazed surface. Recent studies [12,13] have demonstrated that the surface glaze developed is nanocrystalline in nature and such nanostructured glazes provide resistance against high temperature wear. It has also been clear that the formation of glaze with appropriate microstructures cannot always provide the required immunity against high temperature wear. Such glazes with potential to inhibit wear may collapse if the material underneath the glaze layer becomes mechanically, microstructurally and chemically instable. Clearly, the wear resistance is determined not only by the topmost surface glaze, but also by the characteristics of the entire wear affected region.

This work has been designed to obtain detailed structural information of the entire wear affected region of the wearing specimen using scanning electron microscopy (SEM), energy dispersive analysis by X-ray (EDX), transmission electron microscopy (TEM), X-ray diffraction (XRD), positron annihilation (PA) and Mössbauer spectroscopy (MS).

*To whom correspondence should be addressed.
E-mail: hailiang.du@unn.ac.uk

2. Experimental

The compositions of materials used for the experimental work are detailed in table 1. The block sample of dimensions 5 mm × 5mm × 45 mm and the cylinder counterface of diameter 50 mm and length 50 mm were machined from commercial Nimonic 80A and Stellite 6 alloys, respectively. The samples were ground starting at 240 grit through to 1200 grit and then polished at 6 μm and 1 μm diamond paste. The counterfaces were ground down to 1200 grit. Both samples and counterfaces were ultrasonically cleaned in acetone.

All high temperature wear tests were carried out on a high temperature reciprocating wear rig in open air. Details of the high temperature wear rig used have been described previously [1,2]. Basically the rig was a block-on-cylinder arrangement (the cylinder being the counterface and the block being the sample). A variable speed electric motor rotated the shaft and connected counterface (Stellite 6) at various speeds. The samples of Nimonic 80A held against the counterface of Stellite 6 using the sample arm in reciprocating motion, with reciprocation at 3 cycles per minute with a constant stroke of 12 mm. The tests were carried out at a sliding speed of 0.314 m s^{-1}, (this being the speed

Table 1.
Nominal compositions of experimental alloys in wt%.

	Fe	Ni	Cr	Al	Ti	Mn	W	Co	Si	C
Stellite 6	2.5 max	2.5 max	27	–	–	1	5	60	1	1
Nimonic 80A	0.7	75.8	19.4	1.4	2.5	–	–	–	0.1	0.08

of rotation of the counterface) under a load of 7 N at various temperatures.

Both the surface and sub-surface layers of the wear-affected region were characterised at various levels. The evolution of microstructures generated or altered at microscale level was evaluated using SEM. The change in composition profiles were monitored using EDX and the phase contents were identified using XRD. Nanoscale information on the wear damaged area was obtained using mainly TEM.

The samples for positron lifetime measurements were produced at 20, 270, 510 and 750 °C by the described sliding wear test procedure [1,2]. After the wear test isothermal annealing was performed on each sample at 1200 °C. The annealing process was used to facilitate the identification of the crystal defects created by straining.

The positron source was made of carrier free ^{22}NaCl sealed between kapton foils. The activity of the source was $5{\cdot}10^5$ Bq and, as checked by source correction measurements on a nickel single crystals sample, less than 8% of positrons annihilated in the kapton foil. These positrons were taken into account in further evaluations as a source correction and any data given below have been obtained by removing an 8% source correction of 385 ps from the spectra by the POSITRONFIT computer code [14].

Two identical pieces of samples were prepared for positron lifetime measurements at every stage of wear and annealing. The positron source and the two samples were arranged in a sandwich-geometry. All measurements were carried out at room temperature. To ensure that the data represents the glazed layer and not simply the bulk material, additional measurements were performed on the backside of each sample. Since this surface had the same thermal history as the glazed layer, any difference between the two lifetime spectra would attribute to the outcome of the sliding wear. This procedure might also prove that, even though they are fast when coming out of the source, most positrons annihilate in the region of interest.

The positron lifetime spectra were recorded by a conventional fast–fast coincidence system [15]. The system was constructed from BaF_2-based detectors and standard ORTEC electronic units. The spectra were collected in the 4096 channels of a PCA3 multichannel analyzer card (Canberra). The time/channel value was set to 10.3 p and the overall time resolution of the system varied between 198 and 205 ps, determined by the RESOLUTION computer code [14] for each spectrum individually.

In addition to the lifetime measurements, Doppler-broadening measurements were also performed and the width of the annihilation photo-peak was measured. The two parameters (W and S) provided by this method characterise the average electron momentum in samples. Roughly speaking, W represents high momentum electrons, while S indicates the relative intensity of low momentum electrons. Technically, the S-parameter was calculated as the ratio of the integrals for the central 17 channels and that for the 256 channels of the entire annihilation peak. The W-parameter was calculated similarly but instead of the central region, two 80-channels wide regions were chosen from the high momentum wings of the annihilation photo-peak. The results are given below as referenced to a common standard sample. Reference spectra were measured after every Doppler measurement on a common standard sample and each S- and W-parameter were normalised by those of the corresponding parameters of the standard.

For these measurements, an HPGe detector was used with the proper electronics. The resolution of the system was around 1.1 keV at 510 keV.

It should be stated here that high-energy positrons coming from a ^{22}Na-source have an exponential penetration profile. Thus, the information they provide is an average. In pure nickel, the mean penetration depth of positrons is equal to 25.5 microns [16].

CEM spectrum of samples of wear tested at 750 °C were recorded, at room temperature, by conventional Mössbauer spectrometers (WISSEL) working in constant acceleration mode using NUCLEUS PC card as multichannel analyser. The measurements were carried out with a flowing gas (96% He, 4% CH_4) proportional counter and a 57Co(Rh) source of 1.85 GBq activity. Isomer shifts were given relative to α-Fe. The evaluation of Mössbauer spectra was performed by least-square fitting of the lines using the MOSSWINN program [17]. The Mössbauer spectrum gives information about the surface up to maximum 0.3 μm depth.

3. Results

3.1. Wear and friction data

Figure 1 displays the wear data in terms of weight changes on Nimonic 80A/Stellite 6 system as a

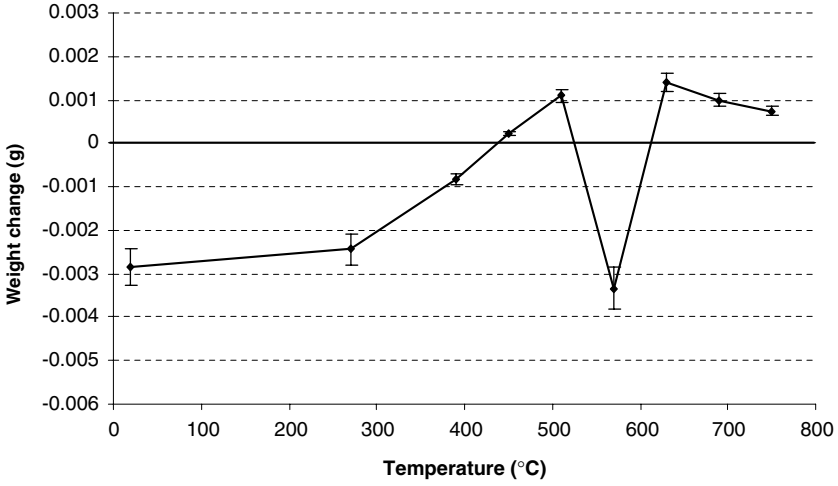

Figure 1. Weight change versus temperature for Nimonic 80A against Stellite 6.

function of temperature under a load of 7 N at 0.314 m/s^{-1} for total sliding distance of 4522 m. Weight changes were extremely low at all temperatures, with the largest mean change being 0.002(4) g at 270 °C. Slight gains were observed for all test temperatures between 450 °C and 750 °C. The wear data at 570 °C shows a departure from the general trend. Repeated experiments confirmed the data at 570 °C needing further attention.

The coefficient of friction values measured during each of the tests showed an initial period of rapid change, before, in many cases, settling down into a 'steady state' situation with reduced variation, as revealed in figure 2. In previous work [2], this was attributed to either the presence of a third body (i.e. debris) or glaze establishing itself at the interface. At 0.314 m s^{-1}, this variation was no more than approximately 12% of the mean value in steady state.

3.2. SEM surface morphologies and XRD results

Figure 3 illustrates the SEM micrographs of wear scar surfaces after 4522 m of sliding at 0.314 m s^{-1} at 20, 270, 510 and 750 °C. It is apparent that after an initial period of severe wear, oxidised debris formed, which left a layer of oxide powder across the surface of the wear scar. As reported in previous work [2], this material seemed to 'smear' at 270 °C, and especially at 390 °C for 0.314 m s^{-1}. At 390 °C and above, the behaviour diverged dramatically. At 450 °C, the debris on the surface showed evidence of particles 'sticking' or sintering together, with one or two isolated patches

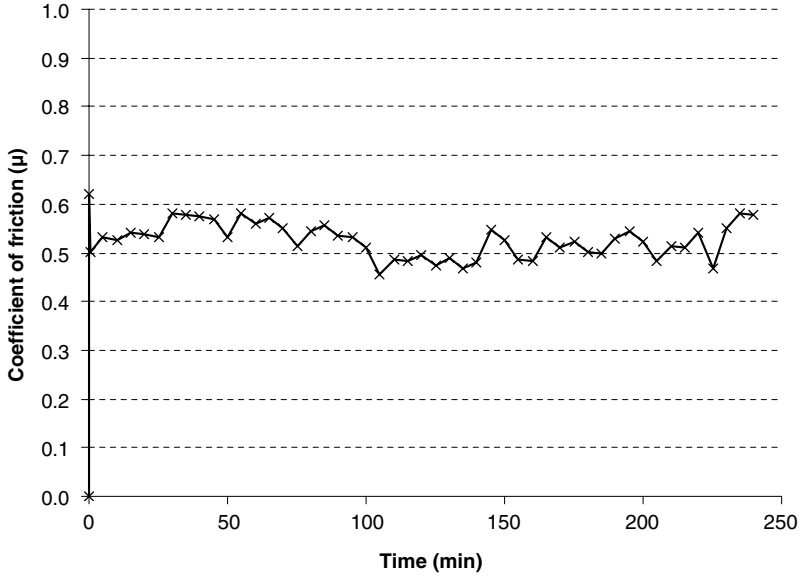

Figure 2. Coefficient of friction versus time for Nimonic 80A versus Stellite 6 at 750 °C.

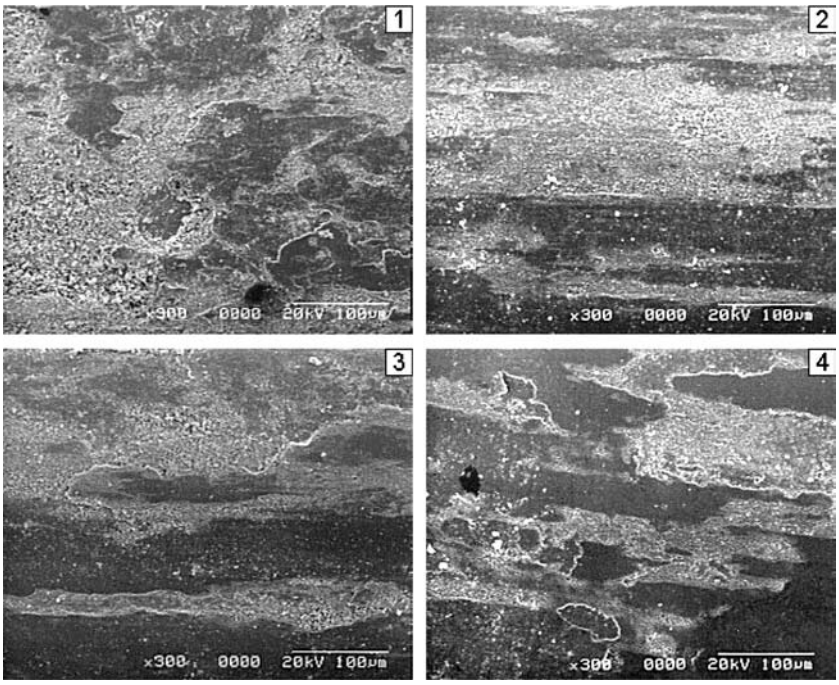

Figure 3. SEM morphologies of worn surface of Nimonic 80A versus Stellite 6.

of glaze-like material observed. At 510 °C and above, glaze formation became increasingly evident, with very low levels of wear.

The EDX analysis for the 0.314 m s^{-1} samples showed that the fine debris covering the surfaces at room temperature, 270 °C and 390 °C consisted of varying levels of nickel, chromium and cobalt, dependent on the area selected. Selection of an area high in fine debris particles gave a higher cobalt level (up to 50%), whilst an area relatively free of particles indicated a higher level of nickel (up to 60%, with cobalt levels falling to less than 10%) from the sample substrate metal beneath, showing no evidence of transfer of metal between the counterface and the sample.

From 450 °C upwards with the debris smearing together and a glaze forming, cobalt levels in glaze-covered regions were higher, although still fairly variable at between 35 and 55%. The levels of nickel detected dropped to less than 10% within the glaze, although some values reached between 15 and 18%, where glaze was patchy and measurement of 'glaze-only' was difficult. Specific analysis of breaks in the glaze showed very high nickel levels, with the glaze having broken away to reveal the Nimonic 80A substrate underneath. Chromium levels in the glaze remained high throughout (30–35%), with substrate levels of chromium remaining at around 25%.

The evaluation of diffractograms (the assignment of XRD reflections to phases) is illustrated in figure 4 for the sample tested at 750 °C. The main fcc pattern is attributed to the bulk Nimonic 80A phase. The additional cubic phase is associated with a solid solution alloy phase in which the concentrations of the alloying elements are different (e.g. Ni content decreases since the lattice parameter increases) from that of Nimonic 80A. Some external elements (e.g. Co and Fe) could be incorporated, which may lead to an increase in the lattice parameter. It is also possible that there is a phase which is somewhat ordered. This phase may be connected to the effect of wear test when a mechanical alloying of the Stellite 6 on the Nimonic surface could occur. In this case a Co–Cr–Ni–Fe– alloy could be formed in correspondence with the EDX analytical results. However, the exact concentration of this alloy cannot be obtained from the XRD analysis. The third component can be well attributed to a $CoCr_2O_4$ oxide which may contain other alloying element (e.g. Fe) as demonstrated by the Mössbauer spectrum, which shows clearly the evidences that iron is incorporated in the alloy phase in the surface, as shown in figure 5. However, the resolution is poor because the iron content is low for the CEM measurement. The spectrum was decomposed into a singlet (S1) reflecting the fcc alloy phase, a doublet (D) associated with paramagnetic highly disordered (amorphous) iron (III)-bearing oxide hydroxide phases and a magnetically split sextet (S2) corresponding to a highly alloyed $Fe(Cr,Ni)_3O_4$ phase.

3.3. TEM results

The selected specimens were characterised by TEM. Figure 6 illustrates a cross-sectional composite transmission electron micrograph of the surface formed

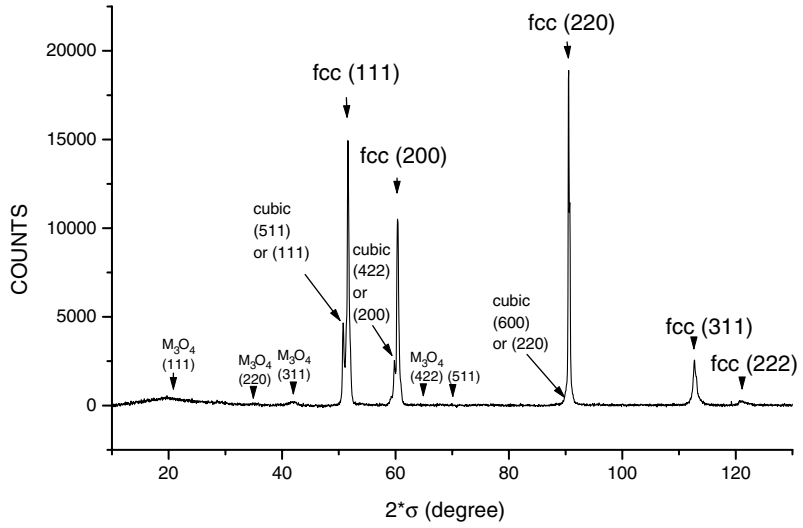

Figure 4. XRD pattern for Nimonic 80A versus Stellite 6 at 750 °C.

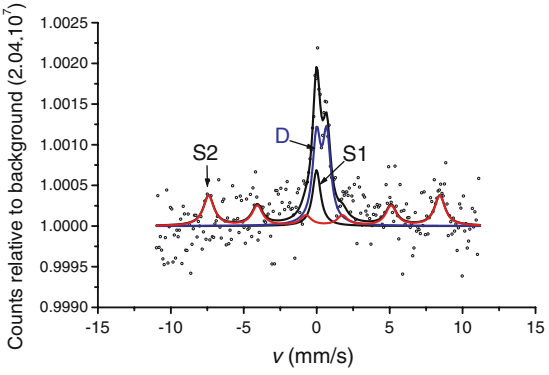

Figure 5. Conversion electron Mössbauer spectrum for Nimonic 80A against Stellite 6 at 750 °C.

during wear test at 750 °C. The micrograph demonstrates the presence of the surface layer (glazed surface), the deformed substrate and the glazed layer/substrate interface. The wear-affected region (total thickness ~3 μm) consisted of three layers—the top most layer (the glaze layer) showed the presence of uniform grain structure of size 5–15 nm; some of the grains displaying contrast—the dislocation density in this area was low. The interfacial layer consisted of grains of size 10–20 nm and had a higher dislocation density. The layer just beneath the interfacial layer showed subsurface deformation and the presence of elongated grains. The structure of the glazed layer and the selected analysis diffraction (SAD) pattern are separately presented in figure 7. The SAD pattern consisted of spots arranged in concentric circles indicating the presence of small grains with high angle boundaries, multiple boundaries and large misorientations (formation of misorientated lattice-fragmentation). The poorly defined irregular boundaries indicate non-equilibrium high-energy configuration. The indexed SAD pattern also revealed the presence of oxides of Ni, Cr

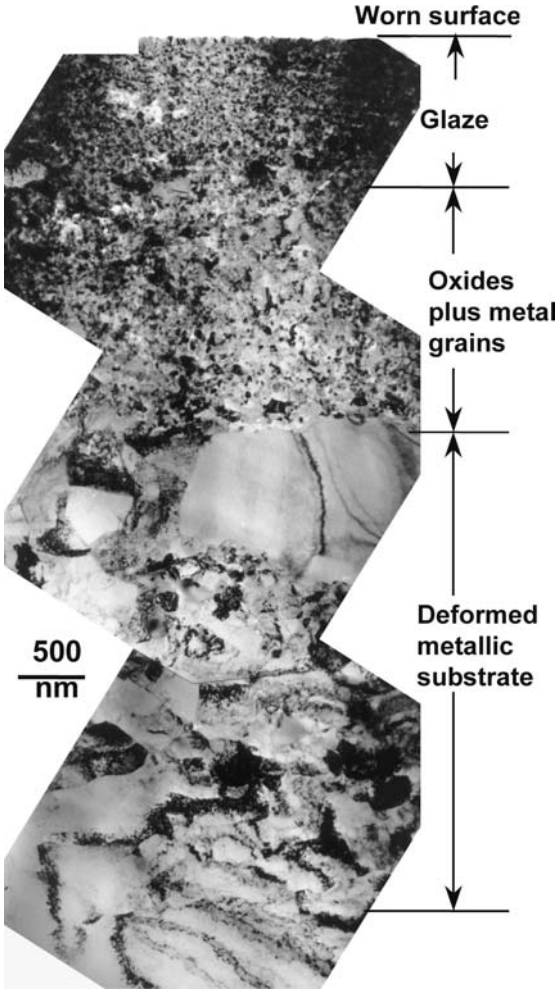

Figure 6. TEM bright field image: wear-induced polycrystalline glaze layer and deformation of substrate.

and Co (indexing not shown here). The dark field images further elaborate on the grain structure of the glazer layer.

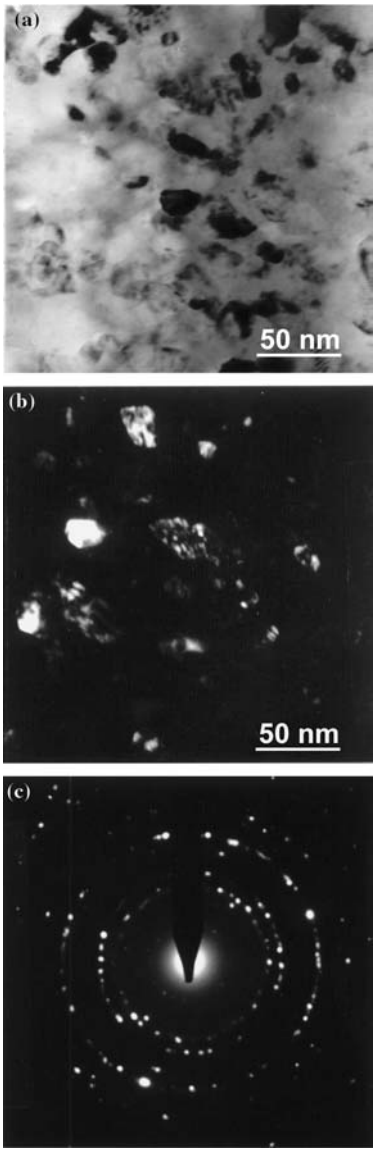

Figure 7. TEM morphological and structural details of glaze layer. (a) Bright field image, (b) dark field image and (c) selected analysis diffraction.

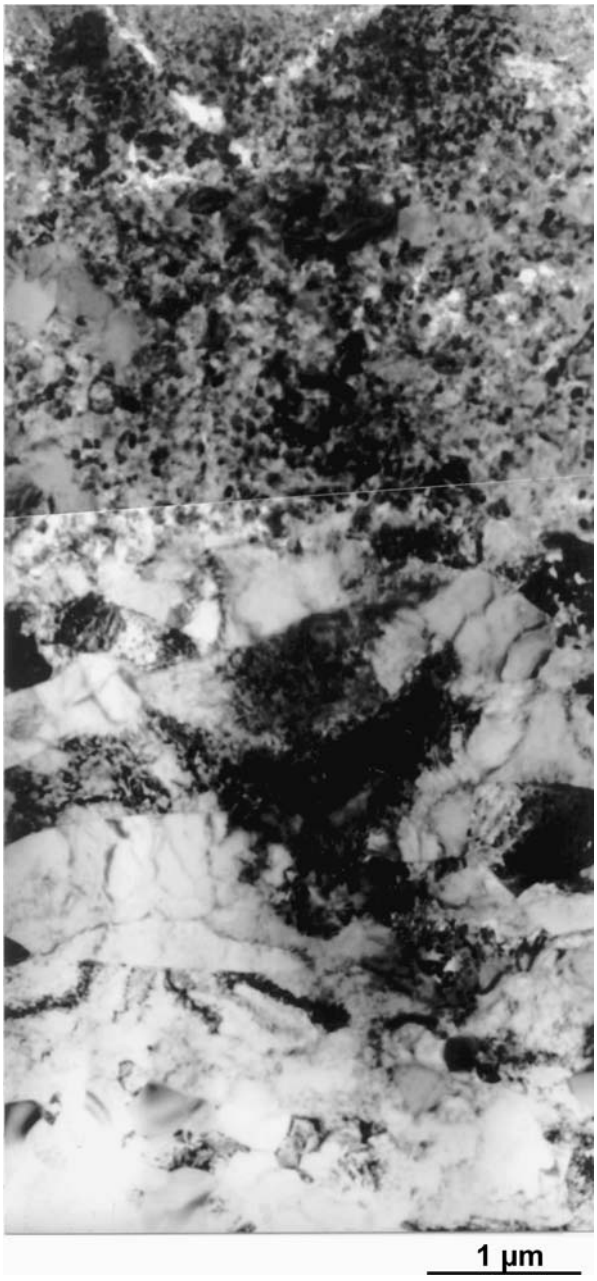

Figure 8. TEM bright field image: wear-induced polycrystalline glaze layer and deformation of substrate.

The occurrence of sub-surface deformation is illustrated in figure 8. Dislocations are observed in the deformed substrate. These dislocations are present as networks inside the deformed (elongated) grains. It was evidenced that shearing deformation took place in the substrate as a response to the sliding process.

3.4. Positron annihilation

All positron data collected from the backsides of all samples, i.e. from unstrained surfaces, were identical. However, the wear affected surfaces provided distinct lifetime and Doppler-broadening parameters demonstrating the effects of the sliding wear. Also these data showed that the glazed layer on the surface of the Nimonic 80A was thick enough to be investigated by an unmoderated positron source.

Three lifetime components were identified in all spectra measured on the worn surfaces. The longest one of these components (around 1800 ps) was easy to identify. It is definitely attributable to the small number of positrons forming positronium atoms at the metal surface having diffused from the bulk to the surface before. The intensity of this component was less than 1.5% and did not vary significantly. As a result, this lifetime component is ignored for further considerations but the other two are discussed in details.

Note, that this component is due to the high specific area of strained surfaces. As neither the nickel single crystal reference sample nor the unaffected surfaces of Nimonic 80A provided this component when measured by the same positron source, we should not consider this as a source correction. However, on the other hand, the large backscatter coefficient of nickel and chromium against kapton [18,19] and the rough surface might explain some positronium formation on strained surfaces.

The longer lifetime component of the two main lifetime components identified in the samples was around 360 ps and its relative intensity was approximately 13%. Neither the lifetime nor the intensity varied with annealing time. The only significant feature of this component was its lifetime value was slightly shorter (by some 15 ± 5 ps) and its intensity a little lower (by 2 ± 0.5%) on the strained surfaces than on the unstrained sides.

The shorter lifetime component appears to be more important than the longer lifetime as indicated in figure 9. In the case of unstrained surfaces, its lifetime stayed around 117 ps with minor alterations. On the other hand, the lifetime measured on the strained surfaces differed remarkably from this value in all cases except the samples treated at 750 °C. The largest difference was measured on the samples tested at 20 °C, where the lifetime varied between 148 and 135 ps with the annealing time. As the temperature of the wear test increased the lifetime value was getting close to 117 ps.

Moreover, this lifetime component reacted notably to the high temperature annealing. The only exception

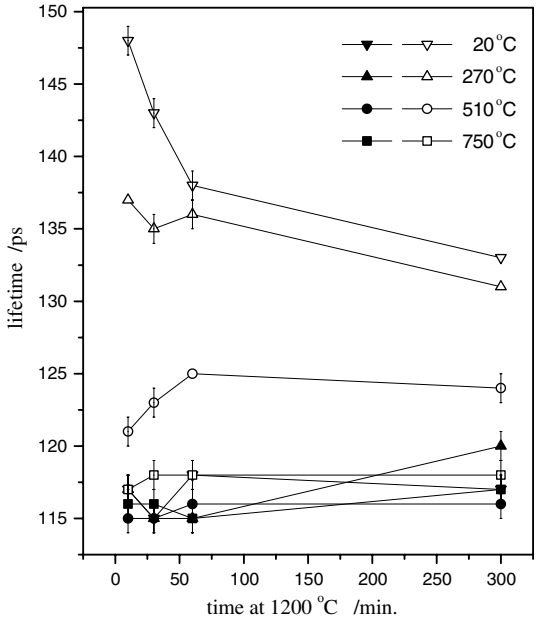

Figure 9. The short positron lifetime, τ_1 measured in samples strained under different wear conditions. Closed symbols mark unstrained surfaces and open symbols represent affected surfaces.

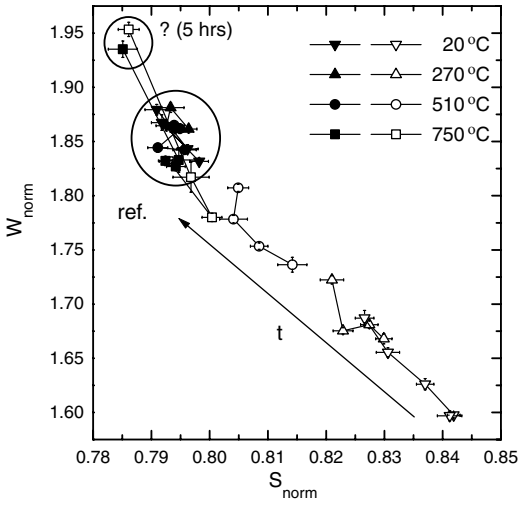

Figure 10. The normalised Doppler-broadening parameters measured on differently treated surfaces of Nimonic 80. Closed symbols indicate un-strained and open symbol represent affected surfaces.

was again the case of 750 °C, where the lifetime remained around 117 ps even after an annealing of 300 min at 1200 °C. It was interesting to notice that this lifetime was, on the effect of annealing, decreased in the samples tested at 20 and 270 °C but increased in the case of wear test at 510 °C.

Doppler-broadening data resembled lifetime data in many respects, as given in figure 10. Both W and S parameter suggested that all of the unstrained samples are identical regardless of the temperature of the wear test whilst the strained surfaces produced different W and S parameters. Again the largest difference occurred on the samples tested at 20 °C and decreased with the temperature of the wear test. The annealing at 1200 °C led to both W and S shifting towards the values measured on the unstrained surfaces. The only break of this tendency was represented by only two points which were measured on the sample treated at 750 °C for 300 min. According to the lifetime data, this sample was completely regular and the irregular points are ignored in further discussions.

4. Discussion

4.1. Observations on glaze surface layer

The formation of nanostructured glazed surfaces during the sliding wear processes can be understood, in a general way, in terms of the mechanisms that were described in previous publications [17,18]. The initial events responsible for generating the glaze layer involve intermixing of the debris generated from the contacting surfaces, oxidation, further mixing (the lack of any composition gradient in the glaze layer indicates efficient intermixing of the components

constituting the layer), repeated welding and fracture and final consolidation.

The next step involves deformation of oxides and generation of dislocations leading to the formation of sub-grains. These sub-grains are then further refined with increasing misorientation giving nano-structured grains with high angle boundaries (a process called fragmentation) and non-equilibrium state indicated by poorly defined and irregular grain boundaries. High internal stress is created inside the grains—dislocation density and arrangement depending on the grain size; smaller grains contained fewer dislocations. The process leads to the formation of high energy grain boundaries with a high defect density [12,13,20–24].

4.2. Observation on sub-surface region

As it was mentioned above the longer positron lifetime (τ_2) did not really related to the wear conditions or the heat treatment. The measured lifetime value (360 ps) could well be developed by positrons annihilating in large three dimensional vacancy clusters [25,26] but positrons trapped at grain boundaries might have a similar lifetime. Comparing positron data with other results (TEM micrographs, XRD spectra), it is considered that the latter assumption is close to the reality. This was confirmed by the stability of this component against high temperature annealing. The constant lifetime and intensity of this component indicated a stable crystal defect that survived even at 1200 °C. Therefore, the grain boundaries could be the ideal candidates.

Thus, the lifetime component τ_2 was formed by positrons having been trapped at the grain boundaries and annihilating there afterwards. The slight differences between the lifetime data of strained and unstrained surfaces can be explained by the formation of nanoscaled grains with larger specific surface areas which is visible clearly in TEM photographs (figure 6).

The effects of sliding wear on the defect structure of samples can be described on the basis of the other lifetime component, τ_1. The value of this lifetime (117 ps), measured on the unstrained surfaces, was close to the bulk-lifetime of pure and defect-free single crystals of nickel (95 ps) and even closer to the lifetime measured formerly in pure polycrystalline nickel (109 ps) [27]. The slightly higher lifetime value can be explained by the high concentration of chromium that makes the nickel crystal 'less dense'. As the additional heat treatments at 1200 °C should remove all vacancies, dislocations and small vacancy clusters from the crystal grains, it is assumed that this lifetime component developed by positrons diffusing in the bulk of the alloy. This is valid only for the unstrained surfaces.

The sliding wear test definitely injected large quantity of dislocations into the crystal structure and these dislocations trap positrons effectively. The lifetime of these positrons differs from those annihilating in the bulk material. However, it is difficult to separate the dislocation lifetime from the bulk lifetime due to the mathematical reasons. They are simply too close to each other. Consequently, in these cases the short positron lifetime (τ_1) is a mixture representing bulk annihilation and positrons trapped in dislocations or other crystal defects. The changes of the lifetime originate from the alterations of the defect structure. Oversimplifying the actual case a little it can be said that a longer lifetime indicate more defects, while the value 117 ps marks the 'perfect' crystal.

Bearing this in mind, it can be stated that the largest amount of crystal defects is formed in the samples at room temperature. These defects are most likely dislocations, according to the well known effects of sliding wear. However, to explain the high lifetime value (130–150 ps), we should assume that the formed dislocations are not simple edge dislocations. According to calculations [28], edge dislocations provide only an 119 ps lifetime for nickel. As the measured lifetime is between the dislocation lifetime and that of a vacancy (175 ps), we assume that some vacancies should have been trapped by the newly formed dislocations. Thus, the free volume in the actual dislocations should be larger than at a simple edge dislocation, which explains the longer lifetime and the considerable positron trapping. Unfortunately, the obtained data are not enough to determine the exact structure of the observed dislocations.

The above statement does not mean that the sliding wear is less harmful at higher temperatures and produces less crystal defects. However, according to the data obtained, the dislocations at high temperatures are mobile enough to reach sinks such as grain boundaries during the wear test, which leads to low density of dislocation at the end of the wear test. The dislocation mobility increases with temperature, which is reflected in the decreasing values of lifetime τ_1. Also Doppler-broadening results indicate that increasing numbers of positrons annihilate in the bulk, i.e., in a surrounding of higher electron momentum, as the temperature of the wear test increases. At 750 °C all dislocations virtually disappear and none remains closed in the sample.

From the high temperature annealing subsequent to the wear test one should expect to remove dislocations from the sample and form a 'perfect' crystal represented by the unstrained surfaces. However, the observed case is slightly different. According to the lifetime data, the annealing process shifts the samples towards an equilibrium state. However, this state is not identical to that represented by the unstrained surfaces. In the samples tested at 20 and 270 °C, the lifetime decreases but not quickly enough and, in fact, in the 510 °C sample it even increases. Doppler-broadening

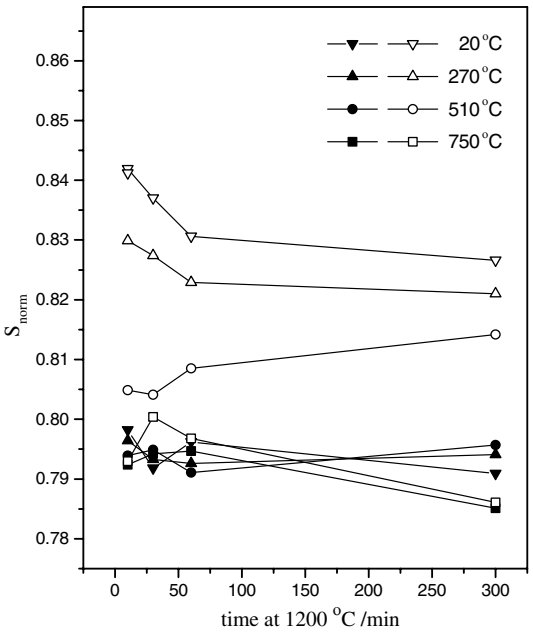

Figure 11. The normalised *S*-parameter as the function of annealing time for the Nimonic 80 samples. Closed symbols indicate un-strained surfaces and open symbols represent affected surface.

parameters show similar 'anomalies' (figure 11) and confirm that the diffusion of dislocations leads to a new 'defect structure' stable enough to exist even at 1200 °C.

To explain the observed 'anomalies' 'crystal defects' stable even at 1200 °C are needed. The presence of nanostructured crystals in the glazing layer may attribute to the anomalies. The preliminary cause for such a crystal defect can be the presence of Cr atoms in the studied Nimonic 80A. The other requirement is the presence of some dislocations, since positron measurements do not indicate the formation of this 'defect' in 750 °C samples. Since Cr atoms demand a bcc structure instead of the available fcc matrix of Ni, they might be able to trap dislocations and form Cr-vacancy clusters. The trapping process does not necessarily stop at the formation of Cr-dislocation complexes but might lead to the formation of ordered or partially ordered regions rich in chromium atoms and vacancies. The vacancies contained by these regions explain the longer lifetime and higher *S*-parameter. Similar processes (e.g., the formation of GP-zones in Al) are well known in other fcc metals and, in those cases, result in the elongation of positron lifetimes [29,30].

Although XRD measurements suggest the formation of a Cr-rich phase very strongly, it should be stated that positrons cannot distinguish this phase from the original Nimonic 80A. The proof for this statement is provided by 750 °C samples, where XRD does but positrons do not see the formation of the mentioned new phase. To find the structure of the observed ordered (or partially ordered) additional measurements needed.

5. Summary

The sliding wear of Nimonic 80A against counterface alloy, Stellite 6, allowed the development of a wear resistant nano-structured glaze layer. The improved wear resistance of such a layer has been attributed to the absence of Hall-Petch softening and the lack of significant degree of work hardening and enhanced fracture toughness of the surface.

Positron lifetime and Doppler-broadening measurements revealed the formation of dislocations in samples wear tested at lower temperatures. At 750 °C the sliding wear was unable to create dislocations in Nimonic 80. Positron measurements suggested that, at 1200 °C, the presence of dislocations might lead to the formation of ordered or partially ordered regions in Nimonic 80A.

Acknowledgments

Grateful acknowledgment to the UK Engineering Physics Science Research Council (EPSRC) is given for financial support to this project. A part of the work was supported by the Hungarian Science Found (OTKA) under the Grant number T034843 and T 043687.

References

[1] P.D. Wood, Ph.D. Thesis "*The Effect of the Counterface on the Wear Resistance of Certain Alloys at Room Temperature and 750 °C*", (Northumbria University, UK, 1997).
[2] S. Rose, Ph.D. Thesis "*Studies of the Large Temperature Tribological Behaviour of Some Superalloys*", (Northumbria University, UK, 2000).
[3] F.H. Stott, D.S. Lin and G.C. Wood, Corrosion Sci. 13 (1973) 449.
[4] M. Johnson, P. Moorhouse and J.R. Nicholls, DTI Industry Valve Project, 61–68, 1990.
[5] J.-N. Aoh and J.-C. Chen, Wear 250–251 (2001) 611.
[6] J. Singh and A.T. Alpas, Metall. Mater. Trans. A 27A (1996) 3135.
[7] M.G. Gee and N.M. Jennett, Wear 193 (1995) 133.
[8] P.D. Wood, P.K. Datta, J.S. Burnell-Gray and N. Wood, Mater. Sci. Forum 251–254 (1997) 467.
[9] A. Wisbey and C.M. Ward-Close, Mater. Sci. Technol. 13 (1997) 349.
[10] J. Jiang, F.H. Stott and M.M. Stack, Wear 203–204 (1997) 615.
[11] X.Y. Li and K.N. Tandon, Wear 245 (2000) 148.
[12] I.A. Inman, S. Datta, H.L. Du, J.S. Burnell-Gray and Q. Luo, Wear 254 (2003) 461.
[13] H.L. Du, P.K. Datta, I. Inman, R. Geurts and C. Kübel, Mater. Sci. Eng. 357 (2003) 412.
[14] P. Kirkegaard, M. Eldrup, O.E. Mogensen and N.J. Pedersen, Comput. Phys. Commun. 23 (1981) 307.
[15] I.K. MacKenzie, in: *Positron Solid-State Physics*, W. Brandt and A. Dupasquier (eds) (North-Holland, Amsterdam, 1983) p. 196.

[16] J. Dryzek and J.E. Dryzek, Phys. Stat. Sol. (A) 179 (2000), 337.
[17] Z. Klencsár, E. Kuzmann and A. Vértes, J. Radioanal. Nucl. Chem. 210 (1996) 10.
[18] I.K. MacKenzie, C.W. Schulte, T. Jackman and J.L. Campbell, Phys. Rev. A7 (1973) 135.
[19] S. Linderoth, H.E. Hansen, B. Nielsen and K. Petersen, Appl. Phys. A33 (1984) 25.
[20] H. Gleiter, Prog. Mater. Sci. 33 (1989) 223.
[21] R.Z. Valiev R.K. Islamgalier and I.V. Alexandrov, Prog. Mater. Sci. 45 (2000) 103.
[22] T.C. Lowe and R.Z. Valiev, JOM 52 (2000) 27.
[23] A.K. Ghosh and W. Huang, in: *Investigations and Applications of Severe Plastic Deformation*, T.C. Lowe and R.Z. Valiev (eds.) (Kluwer Academic Publications, 2000) p. 29.
[24] R.S. Mishra, S.X. McFadden and A.K. Mukherjee, Mater. Sci. Forum 304–306 (1999) 31.
[25] K. Süvegh, A. Domján, A. Vértes, M. El-Sharif, J. McDougall and C.U. Chisolm, J. Electroanal. Chem. 455 (1998) 69.
[26] T. Marek, K. Süvegh, A. Vértes, M. El-Sharif, J. McDougall and C.U. Chisolm, Radiat. Phys. Chem. 58 (2000) 693.
[27] Ch. He, Q. Xu, T. Yoshie, K. Sato and T.D. Troev, Mater. Sci. Forum 445–446 (2004), 105.
[28] E. Kuramoto, T. Tsutsumi, K. Ueno, M. Ohmura and Y. Kamimura, Comput. Mater. Sci. 14 (1999), 28.
[29] C. Szeles and A. Vértes, J. Phys. F: Met. Phys. 17 (1987) 2031.
[30] L. Reich, K. Süvegh, J. Lendvai and A. Vértes, Phil. Mag. Lett. 81 (2001) 145.